Applied Catalysis B: Environmental 224 (2018) 368–375

Contents lists available at ScienceDirect

Applied Catalysis B: Environmental

journal homepage: www.elsevier.com/locate/apcatb

Research Paper

Hydrogenation of sodium hydrogen carbonate in aqueous phase using metal/activated carbon catalysts

Edelmira González[a], Cristian Marchant[a], Catherine Sepúlveda[a], Rafael García[a,*], I.Tyrone Ghampson[b], Nestor Escalona[b], Jose Luis García-Fierro[c]

[a] Departamento de Físico-Química, Facultad de Ciencias Químicas, Universidad de Concepción, Concepción, Chile
[b] Departamento de Ingeniería Química y Bioprocesos, Escuela de Ingeniería, Pontificia Universidad Católica de Chile, Avenida Vicuña Mackenna 4860, Macul, Santiago, 7820436, Chile
[c] Instituto de Catálisis y Petroquímica, CSIC, Cantoblanco, 28049, Madrid, Spain

ARTICLE INFO

Keywords:
Metal/C
Formic acid
Hydrogenation of NaHCO3
CO2 (aq) activation

ABSTRACT

The catalytic hydrogenation of sodium hydrogen carbonate in aqueous phase ($NaHCO_3$) to produce sodium formate (or formic acid) on activated carbon-supported metal (Pd, Ru, Ni, Co and Re) species at 25 °C and 1 bar of hydrogen was studied. The reaction was performed in a semi-continuous flow reactor, and the formate (or formic acid) production was quantified by HPLC, while the gas feed and possible products were quantified by gas chromatography. The catalysts were characterized by N_2 adsorption, Temperature-Programmed Reduction (TPR), X-ray Photoelectron Spectroscopy (XPS), X-ray Diffraction (XRD), Transmission Electron Microscopy (TEM) and carbon monoxide chemisorption. All the catalysts displayed activity in the hydrogenation of sodium hydrogen carbonate and the selectivity to sodium formate was 100%. The Pd/C catalyst presented the highest activity, attributed to stabilized adsorption of reactant which favors the hydrogenation process. The highest intrinsic hydrogenation performance of this metal is related to stability of reduced phases of Pd species observed by XPS and TPR results, favoring the formation of formic acid.

1. Introduction

Carbon dioxide is a natural greenhouse gas which has contributed to moderate temperature and the sustenance of life on earth. However, as a result of the great industrial development of the last two centuries, its concentration in the atmosphere has increased significantly and has been one of the main contributing factors to global warming. Thus, it is reported that the concentration of carbon dioxide has to increase by 2 ppm per year [1]. This can be achieved by the implementation of multiple concepts, including utilizing CO_2 as a raw material in a number of chemical processes. Thermodynamic calculations show that CO_2 is very stable and, as a consequence, its activation and efficient transformation into value-added chemicals is of current interest. According to the report by Song [2], "*CO_2 is not just a greenhouse gas; it is an important source of carbon for obtaining organic compounds and materials*". This author concludes that more research is needed to achieve the efficient and sustainable conversion of CO_2.

One of the most widely reported process of CO_2 utilization is the gas-phase transformation of CO_2 over various heterogeneous catalysts. Specifically, CO_2 has been used in dry methane reforming, various hydrogenation reactions, and as a mild oxidant [3]. However, in most of these cases the reactions are carried out at high temperatures and pressures. As reported by Jessop et al. [4], the use of water as a reaction medium for the hydrogenation of CO_2 allows this molecule to be more readily activated, making its conversion favorable under mild pressure and temperature conditions. The different species present in an aqueous solution of CO_2 are represented by the equilibrium equation (1). Meanwhile, the hydrogenation reaction of sodium hydrogen carbonate in the aqueous phase is represented by equilibrium (2)

$$CO_2(g) + H_2O(l) \rightleftarrows CO_2(ac) \rightleftarrows H^+(ac) + HCO_3^-(ac) \quad (1)$$

$$HCO_3^-(ac) + H_2(ac) \rightleftarrows HCO_2^-(ac) + H_2O(l) \quad (2)$$

Carbon dioxide hydrogenation in the aqueous phase has been reported using homogeneous catalysis and photocatalysis. In homogeneous catalysis, the use of various metal complexes has been reported [5–7]. Federsel et al. used Ru complexes to study the reduction of CO_2 via hydrogen carbonate through an intramolecular transfer of hydrogen [8]. On the other hand, Frank *et* al. [9] employed photocatalytic process for the hydrogenation of the hydrated form of CO_2 (hydrogen carbonate ion). Nevertheless, there is substantial incentive to utilize

* Corresponding author.
E-mail address: rgarcia@udec.cl (R. García).

http://dx.doi.org/10.1016/j.apcatb.2017.10.038
Received 15 May 2017; Received in revised form 2 October 2017; Accepted 13 October 2017
Available online 17 October 2017

heterogeneous catalysts for this process due to the obvious advantages of catalyst separation from the liquid reactant and its reusability

Several metals have been used in different hydrogenation processes, including palladium which is one of the most widely reported. Pd has been used in the hydrogenation of alkenes, hydrogenation of NO and NO_2, hydrogenation of nitrobenzene, benzaldehyde, styrene and selective alkyne hydrogenation [10–13]. Nickel has also received considerable attention. For example, the nickel-catalyzed [Nickel Pincer Complexes] decomposition of formic acid to yield molecular hydrogen and the nickel-catalyzed hydrogenation of bicarbonate as a carbon dioxide mimic has been examined [14]. Chen et al. [15] used a commercially available Ni powder catalyst for CO_2 reduction with $N_2H_4{\cdot}H_2O$ as a reductant. Recently, unsupported nanoporous nickel material was reported by Wang and co-workers [16] for the hydrogenation of carbonates to formic acid in water. Other studies have investigated non-traditional hydrogenation catalysts such as rhenium. Zheng et al. [17] reported the use of ZrO_2- and CeO_2-supported Re catalysts for CO and CO_2 hydrogenation to methanol; furthermore, the Re catalysts were applied to the reactions of formic acid and formaldehyde with hydrogen. Bimetallic Re-based catalysts were used by Yoshino and co-workers [18] for the hydrogenation of carboxylic acids to alcohols at low temperature and under low pressure, while Pritchard et al. [19] utilized supported Pt, Re and Pt-Re catalysts for the hydrogenation of carboxylic acids. In the latter study, the authors explained the catalytic activity results on the basis of synergy between Pt and Re, related to decreasing particle size and H_2-spillover. On the other hand, Wang et al. [20] reported the activity of Ru catalysts dispersed on various supports (γ-Al_2O_3, MgO and activated carbon) in the hydrogenation of CO_2 to form formic acid at 353 K, 5 MPa of H_2 and 8.5 MPa of CO_2 pressures. In this study, the authors highlighted the importance of the surface chemical functionality of the supports on the catalytic activity. Finally, the use of Co complexes as catalysts for the conversion of CO_2 to formate was reported by Jeletic et al. [21]. Despite the strides made, the use of heterogeneous catalysts in carbon dioxide hydrogenation in aqueous phase has received scant attention in the literature. In general, these reports [20,22–26] present a very descriptive catalytic activity, in which Pd and Ru are the most active catalysts. Thus, for heterogeneous catalytic hydrogenation of carbon dioxide in the aqueous phase, there is still insufficient information in order to rigorously rationalize the influence of critical catalyst parameters, such as nature of the active phase, the metal-support interaction and the chemical and textural characteristics of the supports. In the present work, different metallic catalysts supported on activated carbon were evaluated for the aqueous-phase reduction of CO_2 (in the form of sodium hydrogen carbonate) to sodium formate at ambient temperature and pressure. This was done to access the influence of the nature of the active phase. The metallic catalysts include demonstrable hydrogenation active phases such as Pd, Ru and Ni, as well as less-explored active phases like Co and Re.

2. Experimental

2.1. Catalysts preparation

A commercial activated carbon (Darco MRX) purchased from Norit was used as support. In order to eliminate possible presence of metals prior to use, the support was treated with aqueous solution of HNO_3 (1 mol L^{-1}) at 90 °C for 6 h, thoroughly washed with deionized water and dried at 120 °C. The catalysts were prepared by dry impregnation using appropriate amount of metal precursors to obtain a 5 wt.% nominal loading in the final catalyst. As precursors, nitrates were used for Ni and Co, chlorides for Pd and Ru, and ammonium perrhenate for Re. After impregnation, the sample was left at room temperature for 24 h, dried at 110 °C for 12 h and reduced in hydrogen flow for 4 h at temperature ranging from 350 °C and 450 °C depending on the metal and the information obtained by temperature-programmed reduction (TPR).

2.2. Catalytic activity assays

The reaction was carried out in a semi-continuous flow glass reactor at 25 °C. Hydrogen was bubbled to the reactor at atmospheric pressure with a flow of 50 mL min^{-1}. A solution of sodium hydrogen carbonate (100 mL, 1 mol L^{-1}) and 200 mg of catalyst (100 mesh in particle size) were then introduced to the reactor. Liquid samples were extracted as a function of time and the production of sodium formate was analyzed and quantified by HPLC. The presence of gaseous phases, hydrogen, carbon dioxide and the possible presence of carbon monoxide and methane were analyzed online by gas chromatography equipped with TCD using a Carboxen 1000 60/80 packed column. The presence of liquid products other than formate in aqueous solution, such as formaldehyde and methanol, were analyzed by gas chromatography equipped with FID using a Nukol capillary column.

2.3. Catalysts characterization

The textural properties of the catalyst were characterized by nitrogen adsorption at −196 °C by Micrometrics TriStar II 3020 equipment. Prior to the measurements, the samples were outgassed at 300 °C for 2 h. Total pore volume (Vp) was recorded by nitrogen adsorption at a relative pressure of 0.99, while micropore volume (Vo) was determined by the Dubinin–Radushkevich method. Mesopore volume (Vm) was determined by the difference between Vp and Vo.

The reduction temperature of the metal precursors was obtained from temperature-programmed reduction (TPR) measurements carried out in a quartz cell in a system equipped with a TCD. In the experiment, 20 mg of previously dried sample was heated under 5% H_2/Ar flowing at 50 mLmin^{-1} from 25 °C to 1050 °C (heating rate of 10 °C min^{-1}).

The dispersion and particle size of the metallic phase were determined by CO chemisorption and transmission electron microscopy (TEM). The CO chemisorption measurements were performed in Micromeritics ASAP 2020C equipment. Before analysis, the catalysts were reduced "*in situ*" for 4 h under H_2 flow at temperatures between 350 °C and 450 °C, depending on the metal and the information obtained by temperature-programmed reduction (TPR). After reduction, the reactor tube was evacuated at 400 °C to remove the remaining H_2. Finally CO chemisorption analysis using double isotherm methodology was performed at 35 °C with pressure ranges between 0.5–9.5 mmHg. Metal dispersion was calculated assuming a 1:1 stoichiometry of CO:Re [27], CO:Ru [28] and CO:Ni [29,30]. On the other hand, a stoichiometry of 1:2 was assumed for CO chemisorption on Pd [31–33] and Co catalysts [34]. From the CO uptake and the real metal content, the dispersion (D%) and active metal surface (S_M) were calculated. Finally, using the cubic Boudart criteria for geometric shape the particle size (d) was estimated. TEM measurements were carried out in a JEOL JEM 1200 EX II model microscope, in which several photographs of the samples were taken in 50–100 nm scale. From the TEM images the particle size average (d) was determined and then active metal surface (S_M) and dispersion (D%) were obtained.

The chemical nature of the metallic phases and their surface ratios were determined by X-ray photoelectron spectroscopy (XPS) using a VGE scalab 200R electron spectrometer equipped with a hemispherical analyzer operating in a constant pass energy mode, and a non-monochromatic Mg-Ka($h\iota$ = 1253.6 eV, 1 eV = 1.603×10^{-19} J) X-ray source operated at 10 mA and 12 kV. Prior to the analysis, the catalyst samples were reduced *in situ* in a pre-treatment chamber to avoid oxidation of the metallic phase. The reduction conditions were the same as that utilized before the catalytic activity assays. An estimated error of ± 0.1 eV can be assumed for all measurements. Intensities of the peaks were calculated from the respective peak areas after background subtraction and spectrum fitting by a combination of Gaussian/Lorentzian functions. The relative surface atomic ratios were

Table 1
Textural properties and real metal loading of the catalysts.

	S_{BET} ($m^2\,g^{-1}$)	V_P ($cm^3\,g^{-1}$)	V_o ($cm^3\,g^{-1}$)	Vm ($cm^3\,g^{-1}$)	Real metal content (wt. %)
C	664	0.68	0.14	0.54	–
Co/C	627	0.63	0.14	0.49	4.93
Ni/C	658	0.67	0.14	0.53	4.47
Re/C	606	0.61	0.14	0.47	4.33
Pd/C	575	0.58	0.13	0.45	4.48
Ru/C	636	0.64	0.14	0.50	5.06

determined from the corresponding peak areas, corrected with tabulated sensitivity factors with a precision of 7%.

3. Results and discussion

3.1. Textural characterization

Table 1 shows the textural characterization of the carbon support (C) and catalysts from nitrogen adsorption, and the metal content obtained by ICP/MS. The support used displayed a relatively low surface area (S_{BET}) for an activated carbon; however, it presents significant mesoporosity which should facilitate the diffusion of reactants in aqueous solution. Also, Table 1 shows that the textural properties of catalysts were similar to that of the support, indicating that metal impregnation and subsequent thermal treatment did not significantly modify the textural characteristics. In particular, the micropore volume remained unchanged from the support, indicating that the metal species were deposited exclusively in the mesopores. The preferential adsorption of metal ions in the mesopore could either be related to the high concentration of adsorption positions in the mesopore or the diffusional limitation of aqueous metal ions into the micropores. It should be pointed out that there were no obvious differences on the catalyst porosity due to the different metal precursors used for impregnation. The metal content obtained from ICP/MS is similar to the nominal loading value of 5 wt.%, suggesting a good impregnation process.

3.2. TPR results

Fig. 1 shows the TPR profiles obtained for Pd, Re, Ru, Ni and Co precursors supported on activated carbon, and the corresponding support as reference.In this figure, a single peak is observed at 167 °C for PdO reduction to Pd metal [35]. For the Re/C precursor, the broad peak centered at 350 °C with a shoulder at lower temperatures suggests a two-step reduction of ReOx species to Re metal. According to Arnoldy et al. [36] and Escalona and co-workers [37], the shoulder around 313 °C can be attributed to the reduction of ReO_3 to Re°, whereas the principal peak at 350 °C was attributed to the reduction of Re_2O_7. For Ni/C precursor, there are three signals, at 306 °C, 352 °C and 418 °C: the first peak is attributed to the reduction of highly dispersed NiO to Ni metal particles with low interaction with the support; the peak at 352 °C is related to the reduction of Ni(II) species with moderate interaction with the support; and the high-temperature peak at 418 °C corresponds to Ni(II) species with strong interaction with the support [38]. For the Co/C precursor, a broad peak from 350 °C to 450 °C with amaximum at 439 °C can be observed which corresponds to the two-step reduction of Co oxide species ($Co_3O_4 \rightarrow CoO \rightarrow Co$)[39–41]. The Ru/C precursor displays two reduction peaks, in which the first peak at 152 °C is assigned to the reduction of Ru(III) species to Ru^0, and the second peak observed at 216 °C is attributed to the reduction of Ru(IV) species to Ru^0, according to Betancourt et al. [42]. The TPR results show different level of interaction between the different metallic functions and the activated carbon support. It can be concluded that the optimum reduction temperature for the supported metal precursors are: 430 °C for Ni/C, 450 °C for Co/C, 360 °C for Re/C, 220 °C for Ru/C and 180 °C for Pd/C. Fig. 1 also shows low hydrogen uptake between 550 °C to 850 °C associated with the reduction of certain surface functional groups on the support.

3.3. Transmission electron microscopy and CO chemisorption results

Fig. 2 show the TEM images of the catalysts, while Fig. 3 shows the mean particle diameter and a measure of its corresponding particle size distribution (represented by the length of the black arrows). The mean particle sizes (blue circles) increase in the order: Ru/C (3 nm) < Ni/C (4 nm) < Pd/C (5 nm) < Re/C (8 nm) < Co/C (14 nm). The Ru/C catalyst exhibits the narrowest distribution with particle size between 2 and 7 nm, followed by the Ni/C catalyst with sizes between 2 and 12 nm, and then the Pd/C catalyst with a distribution between 2 and 15 nm. Broader size distributions were observed for Re/C and Co/C catalysts (2–30 nm).

In Table 2 the results of dispersion (D%), particle size (d) and metallic surface (S_M) obtained by CO chemisorption and TEM analysis for the catalysts are summarized. As can be seen, these two techniques generally presented the same trends. The discrepancy of the values obtained for the Re/C catalyst could be linked to general instability of Re species during microscopic analysis [43].

3.4. XPS results

In Table 3 the XPS results are summarized. It is observed that the surface chemistry of the support has not been modified after the preparation process of the catalysts. Practically, the same signals are observed at the same binding energies of the C 1 s and with very similar relative abundances. According to the bibliography [44–47], the binding energies at 284.8 eV is related to aromatic graphitic structures; the 286.2 eV signal is related to alcoholic or phenolic surface functional groups; the 287.7 eV peak corresponds to carbonyl groups; and finally the 289.2 eV signal is related to carboxylic surface functional groups. The most relevant result from the XPS analysis is that only metallic species were present on Pd/C and Ru/C catalysts. In contrast, for the Re/C, Ni/C and Co/C catalysts, metal oxide species were also observed in addition to their metallic counterparts, as similarly observed by Passos et al. [48] and Sun and co-workers [49]. This reflects different ease of reducibility of Pd/C and Ru/C catalysts compared to the Re/C, Ni/C and Co/C catalysts, which might have implications on the catalytic activity.

The surface atomic ratios derived from XPS analysis can be used to compare dispersion of catalysts. However, there were no correlation between the dispersion trend obtained from TEM and CO chemisorption measurements and the surface atomic ration from XPS analysis. This is because while CO chemisorption (and to a lesser extent TEM) probes active metallic phases, the XPS surface atomic ratio represents all surface species associated with the elements that are accessible by X-ray photons. Thus, while the data appear to show a relative predominance of Co and Ni species on the support (in comparison to Re, Pd and Ru), CO chemisorption results indicate that most of these species probably corresponds to inactive metal oxide particles. In Fig. 4, the experimental (XPS) atomic surface ratio and the nominal (Metal/Support) atomic ratio (calculated from real metal content given in Table 1) for the supported catalysts are compared. As can be seen for Pd/C and Ru/C catalysts, the XPS atomic surface ratios are lower than nominal atomic surface ratios, suggesting that part of the metal is dispersed in the porous structure of the support and, as a consequence, were not accessible by the X-ray photons. In fact, smaller particles characterized by CO chemisorption and TEM could be located inside the mesoporous structure of the support. On the other hand, Ni/C, Re/C and Co/C catalysts present a slightly higher XPS atomic surface ratio than the corresponding nominal ratio. These results suggest the enrichment in Ni, Re and Co species on the external surface of the carbon support. It

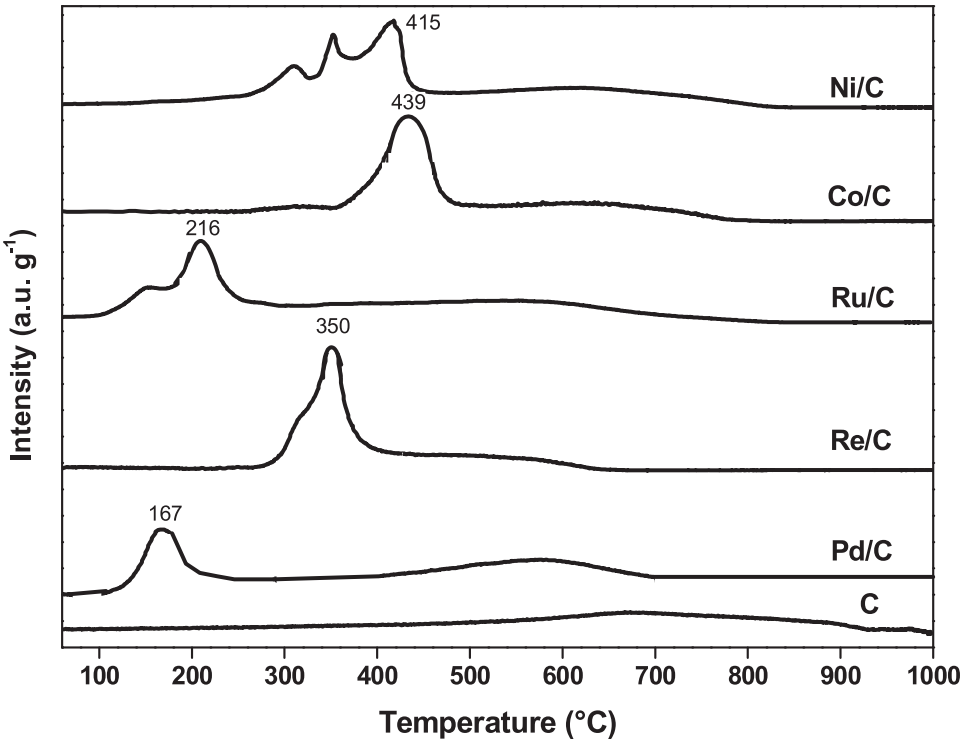

Fig 1. TPR profiles of support and catalysts.

could also be due to overestimation of the XPS surface ratio due to large particle size, especially for the Co/C catalyst. The overestimation of the atomic surface ratio has been previously reported for carbon-supported catalysts [50].

3.5. Catalytic activity results

In all the catalytic activity essays performed, no gaseous (CO and CH_4) products were detected under the experimental conditions used. In addition, neither methanol nor formaldehyde was detected. Due to the fact that all reactions were carried out at room temperature and atmospheric hydrogen pressure, the conversion of $NaHCO_3$ were relatively low. The values vary from 2.0% on the least active catalyst (Co/C) to about 11% on the most active catalyst (Pd/C). Nevertheless, the low activity makes it possible to perform quantitative analysis of reaction rates. The catalytic activity results are shown in Fig. 5. The activity is expressed as moles of $NaHCO_2$ produced per gram of catalyst, and is plotted as a function of time in Fig. 5. It can be observed that the catalytic activity decrease in the order: Pd/C > Ru/C > Ni/C > Re/C ≈ Co/C. The production of $NaHCO_2$ was similarly observed to be highest on Pd/C and Ru/C catalysts by Wrighton et al. [23]. The highest $NaHCO_2$ yield obtained on Pd/C catalyst is attributed to the large hydrogenation capacity of Pd, as has been extensively reported in other hydrogenation reactions [51–54]. The different catalytic activity of metals can be related to the degree of reducibility and the adsorption capacity of a molecule on a metal surface associated to the energy of the "*d*" band center of electronic states in the metal [55,56]. The catalysts with the highest proportion of reduced active phases (Pd and Ru), according to TEM and XPS results, were the most active. On the other hand, the higher activity of Pd/C than Ru/C may be related to differences in their surface electronic properties. A higher *d*-band center (with respect to the Fermi level) corresponds to an increase in energy (relative to the Fermi level) and a subsequent decrease in state filling (d-σ)*. This means that the metal-adsorbate (H_2) is less destabilized, which generates a stronger interaction between the metal and the adsorbate (H_2). Correlation between the *d* band center and the energy of adsorption is well-documented. A major *d*-band center (eV), as is the case of Pd [57], leads to a stronger bond with H_2, but not so strongly that it destabilizes this bond. This allows the hydrogenation process of $NaHCO_3$ to be carried out at a faster rate. For the active phases, which in the experimental conditions used, are in reduced state (Pd and Ru), the activation of $NaHCO_3^-$ species could take place by adsorption on reduced metallic phases, i.e. by interaction between the electron densities (d-orbital) of the reduced metallic phases with the carbon electron deficient center of $NaHCO_3$. The lower activity of Ni/C, Co/C and Re/C catalysts could be due to the following factors. First, the partial oxidation of these metals during the reaction, decrease the reduced active sites available on the surface. And second, the lower energy of the "d" band center of electronic states in the Ni, Re and Co metals.

The specific rate (r_s) for the formate yield is shown in Fig. 6. This is calculated from the initial slope (r) of Fig. 5 according to the following equation:

$$r_s = \frac{r}{S_M}$$

Where "r" is the initial rate of $NaHCO_2$ production per gram of catalyst per time (mmol $NaHCO_2/g_{cat}$·h) and S_M is the active phase metal surface (m^2/g_{cat}) obtained from TEM results. It is clearly observed that the Pd/C catalyst displayed the highest intrinsic rate due to its highest intrinsic hydrogenation capacity. On the other hand, the supported Ru, Ni, Re and Co catalysts presented similarly low intrinsic activity. These results further illustrate the unique ability of Pd sites to transform $NaHCO_3$ to $NaHCO_2$. As was previously explained, the stabilized adsorption of the reactant on the surface of Pd sites favors hydrogenation and led to Pd/C to be the most effective catalyst. The values of normalized initial rate in h^{-1} per metallic active sites shown in Fig. 6 are compared with the initial turnover rate (in h^{-1}) reported previously by Wrighton et al. (23) for the same reaction and under similar experimental conditions. The authors reported TOF values from 0.02 to 35 h^{-1} for supported Pd catalysts. However, it should be noted that these values are not fully comparable. The values shown in Fig. 6 are expressed in $NaHCO_2$ entities per surface metal atoms (active sites) per hour, while the values reported by Wrighton and coworkers are expressed in HCO_2^- ions produced per total Pd atom per h. Despite this last observation, the results obtained are of the same order of

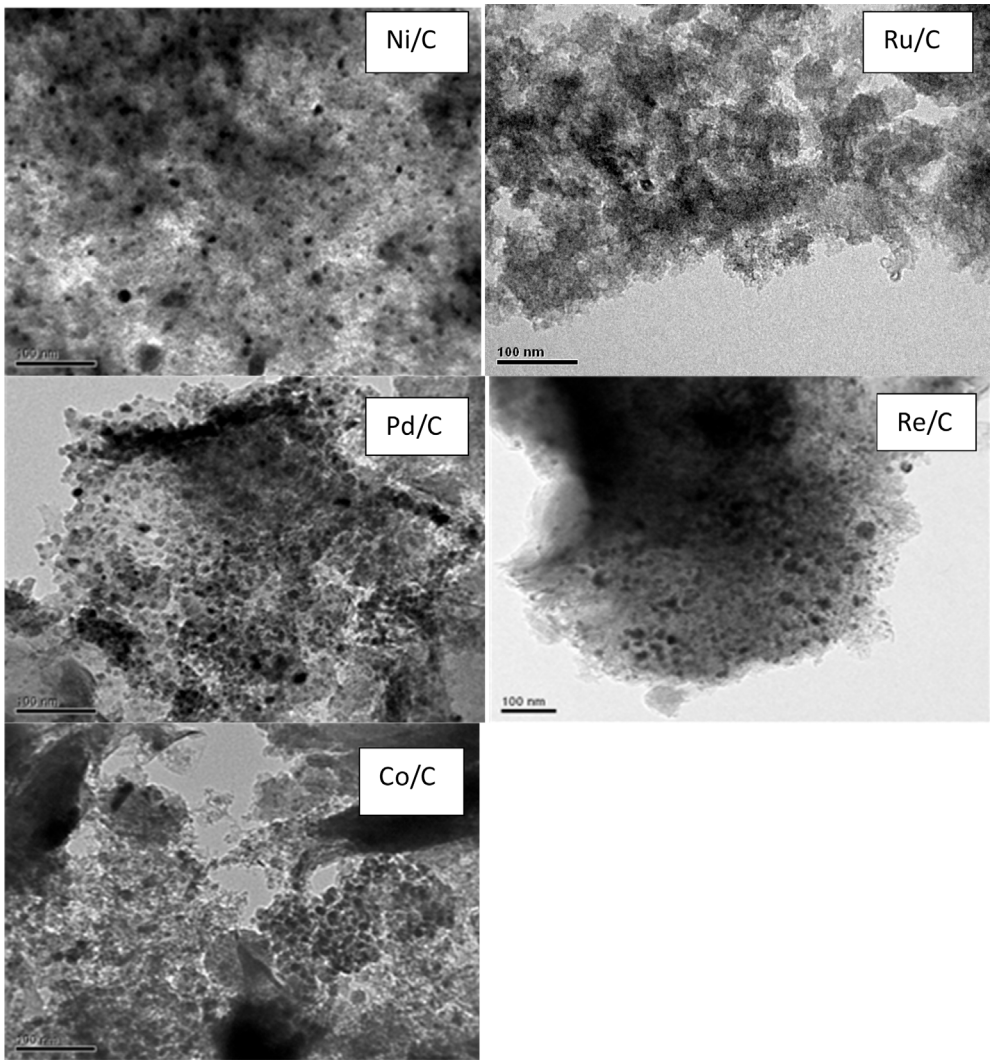

Fig. 2. TEM micrograph of the catalysts.

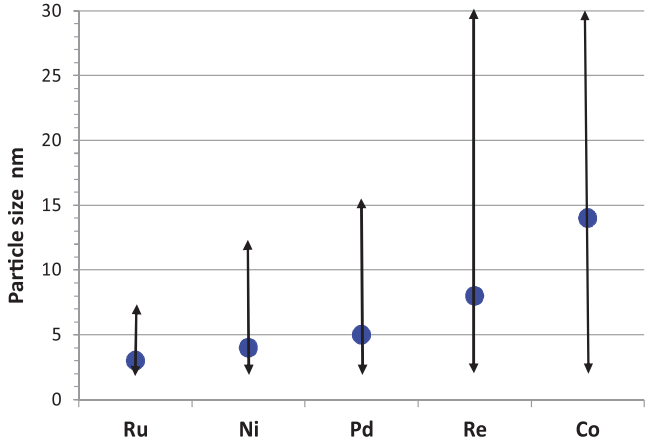

Fig. 3. Particle size and particle size distribution of the supported metal catalysts.

magnitude as those reported in the bibliography.

The stability of the catalysts was tested by reusing the catalysts in multiple runs. After the first reaction, the excess $NaHCO_2$ solution is removed, and the catalyst is repeatedly washed with HPLC grade water while being kept in the reactor. The catalyst is then kept under hydrogen flow at 318 K overnight. A second reaction cycle is carried out by introducing a new solution of $NaHCO_3$ into the reactor after which the catalytic activity is measured at the same previously mentioned conditions. These procedures were repeated three times for each catalyst recycling measurement. Fig. 7 shows that Pd/C and Ru/C catalysts were stable after three runs and then slightly decreased by 10% after the 4th run. In contrast, the activity of Ni/C, Re/C and Co/C catalysts decreased after the first recycle, and continuously decreased afterwards to around 80% of the initial activity for Ni/C and Co/C catalysts and 70% for Re/C catalyst. This is most likely related to the susceptibility of the metallic active phase to oxidation. Noble metal catalysts such as Pd and Ru are less prone to oxidation than non-noble metal transition metal such as Ni, Co and Re. Another possible explanation for the more drastic decrease in activity of the Ni/C, Co/C and Re/C catalysts could be active phase leaching in the reaction medium.

Table 2
Results of catalysts dispersion (D), particle size (d) and metallic surface (SM) obtained by CO chemisorption and TEM.

Catalyst	TEM			CO chemisorption			
	D (%)	d (nm)	S_M ($m^2\ g^{-1}$ cat)	CO uptake ($\mu mol\ g^{-1}$)	D (%)	d (nm)	S_M ($m^2\ g^{-1}$ cat)
Ru/C	25.2	3	122.5	283	55.0	1.5	268
Co/C	5.9	14	40.1	36	8.5	9.7	58
Pd/C	17.6	5	78.5	72	17.0	5.5	76
Re/C	11.7	8	28.7	98	43.0	2.2	106
Ni/C	19.2	4	127.6	111	15.0	6	100

Table 3
Binding energies (eV) and atomic Surface ratios of M/carbon catalysts.

BindingEnergies (eV) and (%)			AtomicSurface Ratio
Support C_{1S}	Active phase		M/C
284.8 (75)	Co/C	77.9(76)	0.0123
286.2 (15)	$2p_{3/2}$	780.4(24)	
287.7 (6)			
289.2 (4)			
284.8 (75)	Ni/C	853.5(34)	0.0101
286.3 (15)	$2p_{3/2}$	855.5(66)	
287.7 (5)			
289.2 (5)			
284.8 (74)	Re/C	41.6(82)	0.0037
286.2 (17)	$4f_{7/2}$	45.4(18)	
287.7 (6)			
289.2 (3)			
284.8 (74)	Pd/C	335.6	0.0031
286.2 (17)	$3d_{5/2}$		
287.7 (5)			
289.2 (4)			
284.8 (72)	Ru/C	280.5	0.0038
286.2 (15)	$3d_{5/2}$	(461.8)	
287.7 (6)	($3p_{3/2}$)		
289.2 (7)			

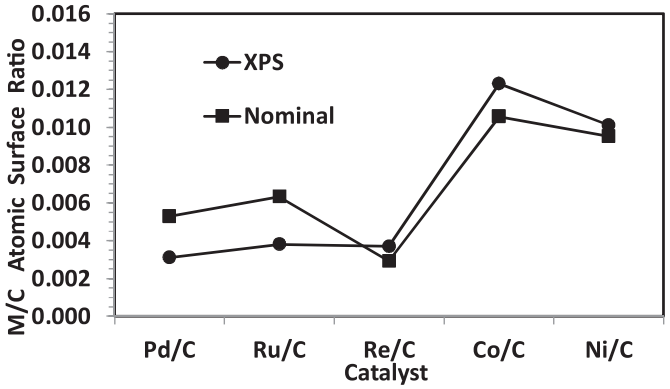

Fig. 4. Surface atomic ratio: comparison of the experimental (XPS) with the nominal values.

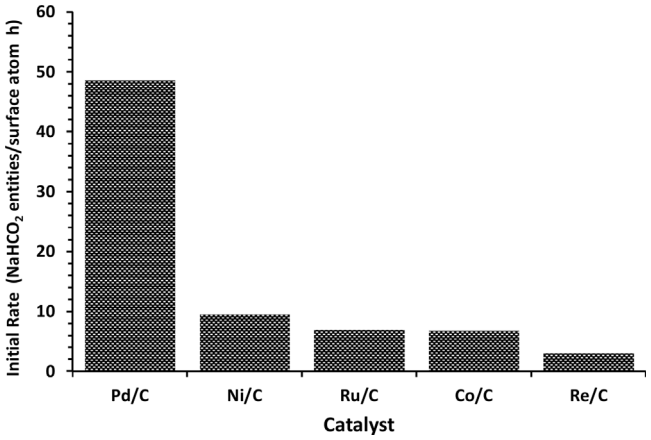

Fig. 6. Normalized initial rate of the catalysts.

The spent catalysts after the fourth recycles were characterized by H_2-TPR and shown in Fig. 8. No hydrogen consumption peaks associated with Pd and Ru species were observed for the Pd/C and Ru/C catalysts, respectively, indicating that the active phases are still in the reduced state even after four recycling tests. Conversely, the TPR profiles of the Ni/C, Co/C and Re/C catalysts show hydrogen consumption peaks at the same reduction temperature (even though the peaks were less intense) as that of the corresponding precursors (see Fig. 1), which confirms that the loss of catalytic activity of these systems could be attributed to the formation of the respective oxidized phases.

4. Conclusions

It has been demonstrated that the reduction of $NaHCO_3$ in aqueous phase and at ambient temperature and hydrogen pressure conditions can be catalyzed by metals supported on activated carbon. The only product detected was $NaHCO_2$. The $NaHCO_2$ yield per mass of catalyst followed the order, Pd/C > Ru/C > Ni/C > Re/C ≈ Co/C, which was related to the nature of active phase present. Nevertheless, when the catalytic activity is expressed as the initial reaction rate of $NaHCO_2$ formed normalized by number of surface metallic atoms, the sequence in catalytic activity change to Pd/C > Ni/C > Ru/C ≈ Co/C > Re/

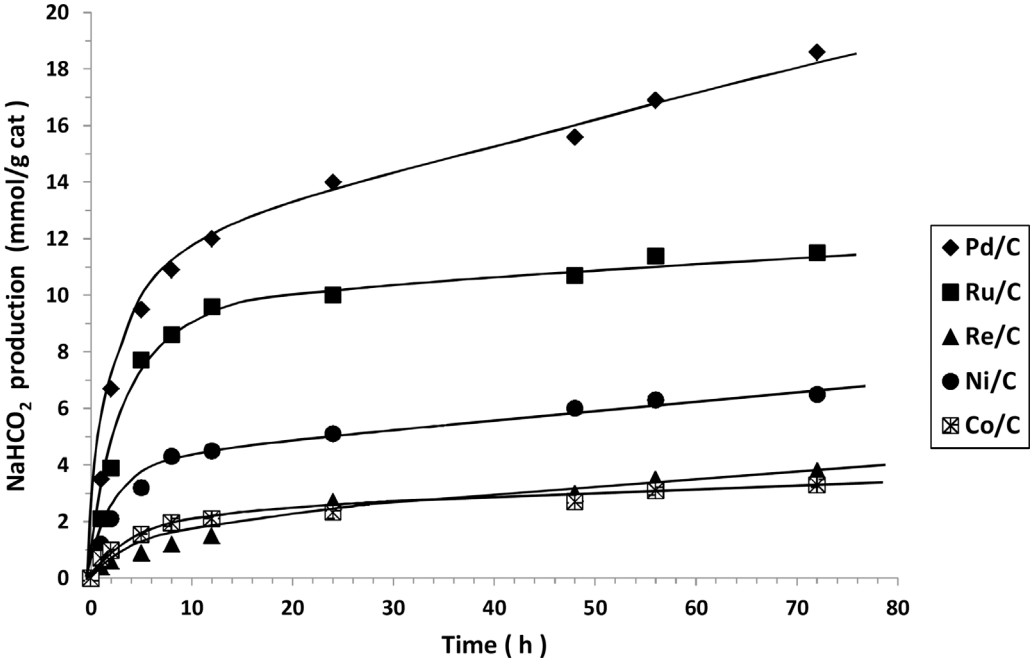

Fig. 5. Catalytic activity expressed as $NaHCO_2$ production.

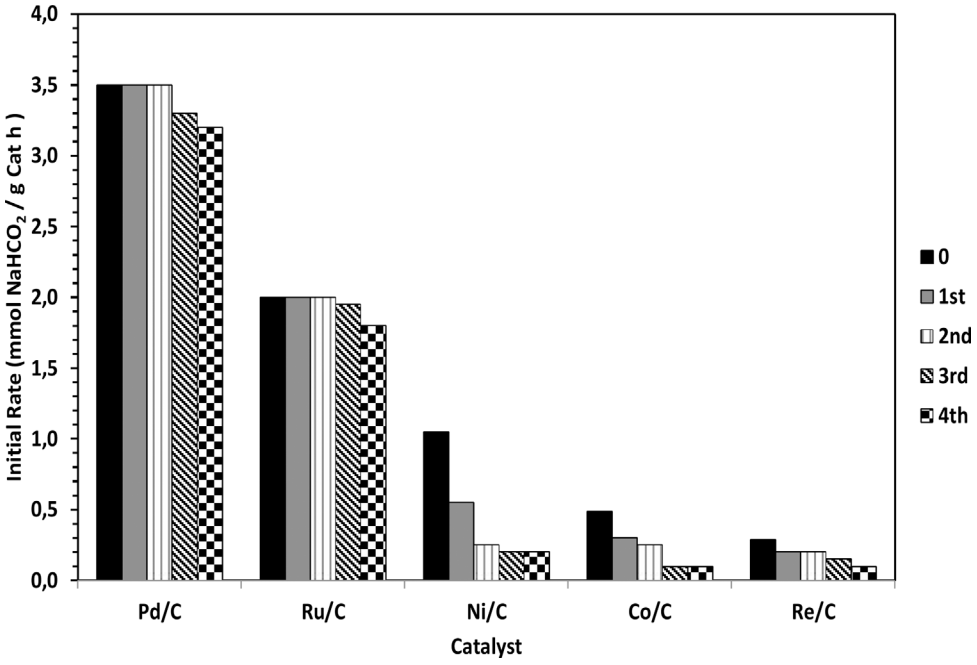

Fig. 7. Initial rate of $NAHCO_2$ formation for recycled runs.

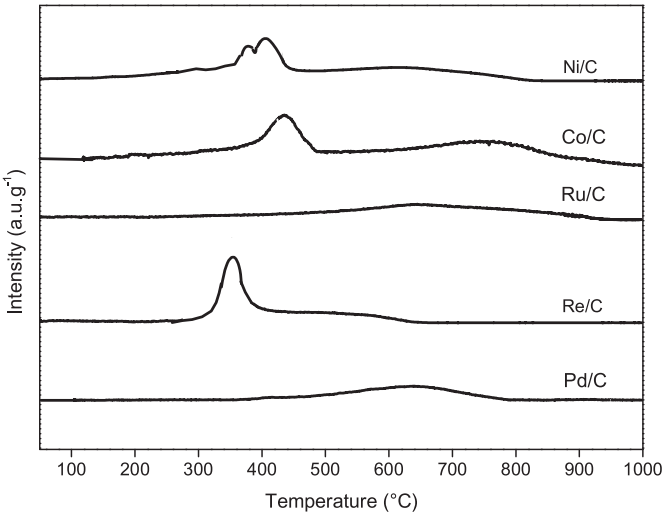

Fig. 8. TPR profiles of spent catalysts after fourthrecycle.

C. This behavior suggests that the catalytic activity does not only depend on the nature of active phase but also on the intrinsic hydrogenation capacity of the elements due to surface electronic properties. As expected, these results confirm the higher hydrogenation capacity of the Pd/C catalyst compared to the other catalysts in the hydrogenation reaction of sodium hydrogen carbonate.

Stability tests of the catalysts confirmed the higher resistance of noble metallic (Pd and Ru) catalysts to oxidation in comparison to non-noble transition metal (Re, Ni and Co) catalysts. This was supported by TPR results which showed significant hydrogen consumption peaks of spent Re/C, Ni/C and Co/C catalysts, while Pd/C and Ru/C catalysts displayed no such peaks.

Acknowledgments

This research was supported by CONICYT-Chile from FONDECYT N°1150953 and FONDEQUIP EQM150103 grants.

Appendix A. Supplementary data

Supplementary data associated with this article can be found, in the online version, at http://dx.doi.org/10.1016/j.apcatb.2017.10.038.

References

[1] R. Lal, Energy Environ. Sci. 1 (2008) 2104–2109.
[2] Chunshan Song, Catal. Today 115 (2006) 2–32.
[3] W. Wang, S. Wang, X. Ma, J. Gong, Chem. Soc. Rev. 40 (2011) 3703–3727.
[4] P.G. Jessop, F. Joó, C.C. Tai Coord, Chem. Rev 248 (2004) 2425–2442.
[5] J.C. Tsai, K.M. Nicholas, J. Am. Chem. Soc. 114 (1992) 5117–5124.
[6] P.G. Jessop, T. Ikariya, R. Noyori, Chem. Rev. 95 (1995) 259–272.
[7] X. Yin, J.R. Moss, Coord. Chem. Rev. 181 (1999) 27–59.
[8] C. Federsel, R. Jackstell, A. Boddien, G. rLaurenczy, M. Beller, ChemSus Chem. 3 (2010) 1048–1050.
[9] Z. Goren, I. Willner, A.J. Nelson, A.J. Frank, J. Phys. Chem. 94 (1990) 3784–3790.
[10] R. Johnstone, J. Liu, L. Lu, D. Whittaker, J. Mol. Catal. A: Chem. 191 (2003) 289–294.
[11] C. Barroo, S.V. Lambeets, F. Devred, T.D. Chau, N. Kruse, Y. De Deckerbc, T. Visart de Bocarmé, New J. Chem. 38 (2014) 2090–2097.
[12] Y. Wanga, Y. Denga, F. Shi, J. Mol. Catal. A: Chem. 395 (2014) 195–201.
[13] D. Teschner, J. Borsodi, Z. Kis, L. Szentmiklósi, Z. Révay, A. Knop-Gericke, R. Schlögl, D. P. Sautet Torres, J. Phys. Chem. C 114 (2010) 2293–2299.
[14] S. Enthaler, A. Brck, A. Kammer, H. Junge, E. Irran, S. Glak, Chemcatchem 7 (2014) 65–69.
[15] F. Chen, G. Yao, Z. Huo, F. Jin, RSC Adv. 5 (2015) 11257–11260.
[16] T. Wang, D. Ren, Z. Huo, Z. Song, F. Jin, M. Chen, Green Chem. 19 (2017) 716–721.
[17] X. Zheng, Q. Zaihu, H. Hideshi, Chem. Soc. Jpn. 64 (1991) 3432–3437.
[18] K. Yoshino, Y. Kajiwara, N. Takaishi, Y. Inamoto, J. Tsuji, J. Am. Oil Chem. Soc. 67 (1990) 21–24.
[19] J. Pritchard, A. Ciftci, M. Verhoeven, E. Hensen, E. Pidko, Catal. Today 279 (2017) 10–18.
[20] C. Hao, S. Wang, Maoshuai Li, L. Kang, X. Ma, Catal. Today 160 (2011) 184–190.
[21] M.S. Jeletic, M.T. Mock, A.M. Appel, J.C. Linehan, J. Am. Chem. Soc. 135 (2013) 11533–11536.
[22] B. Chen, C. Shi, Y. M.Crocker, A. Wang, Appl. Zhu, Catal B: Environ. 132-133 (2013) 245–255.
[23] C.J. Stalder, S. Chao, D.P. Summers, M.S. Wrighton, J. Am. Chem. SOC 105 (1983) 6318–6320.
[24] H. Wiener, J. Blum, H. Feilchenfeld, Y. Sasson, N. Zalmanov, J. Catal. 110 (1988) 184–190.
[25] I. Willner, D. Mandler, J. Am. Chem. SOC 111 (1989) 1330–1336.
[26] B. Wu, Y. Gao, F. Jin, J. Cao, Y. Du, Y. Zhang, Catal. Today 148 (2009) 405–410.
[27] J. Okal, Appl. Catal. A 287 (2005) 214–220.
[28] X. Huoa, D.J. Van Hoomissenb, J. Liua, S. Vyasb, T.J. Strathmann, Appl. Catal. B: Environ. 211 (2017) 188–198.
[29] A.B. Dongil, I.T. Ghampson, R. García, J.L.G. Fierro, N. Escalona, RSC Adv. 4 (2016) 2611–2623.
[30] T.V. Choudhary, C. Sivadinarayana, C.C. Chusuei, A. Klinghoffer, D.W. Goodman, J. Catal. 18 (2001) 9–18.

[31] P. Canton, G. Fagherazzi, M. Battagliarin, F. Menegazzo, F. Pinna, N. Pernicone, Langmuir 18 (2002) 6530–6535.
[32] F. Menegazzo, M. Signoretto, T. Fantinel, F. Pinna, P. Canton, N. Pernicone, Sciences At CàFoscari (2012) 87-94.
[33] H. Sato, T. Mameda, K. Nakai, T.Y. Misaki Haruyama, S. Sonobe, T. Kubota, Y. Okamoto, T. Sugimura, Res. Chem. Intermed. 42 (2015) 31–45.
[34] A.H. Lillebø, E. Patanou, J. Yang, E.A. Blekkan, A. Holmen, Catal. Today 215 (2013) 60–66.
[35] X. Liu, X. Wang, G. Xu, Q. Liu, X. Mu, H. Liu, J. Mater. Chem. 3 (2015) 23560–23569.
[36] P. Arnoldy, E.M. Van Oers, O.S.L. Bruinsma, V.H.J. De Beer, J.A. Moulijn, J. Catal. 93 (1985) 231–245.
[37] N. Martínez, R. García, J.L.G. Fierro, C. Wheeler, R.N. Austin, J.R. Gallagher, J.T. Miller, T.R. Krause, N. Escalona, C. Sepúlveda, Fuel 186 (2016) 112.
[38] X.H. Lu, X.L. Wei, D. Zhou, H.Z. Jiang, Y.W. Sun, Q.H. Xia, J. Mol. Catal. A: Chem. 396 (2015) 196–206.
[39] Y. Su, Y. Zhu, H. Jiang, J. Shen, X. Yang, W. Zou, J. Chen, C. Li, Nanoscale 6 (2014) 15080–15089.
[40] A. Martínez, C. López, F. Márquez, I. Díaz, J. Catal. 220 (2003) 486–499.
[41] O. Ducreux, B. Rebours, J. Lynch, M. Roy-Auberger, D. Bazin, Oil Gas J. 64 (2009) 49–62.
[42] P. Betancourt, A. Rives, R. Hubaut, C.E. Scott, J. Goldwasser, Appl. Catal. A 170 (1998) 307–314.
[43] N. Escalona, M. Vrinat, D. Laurenti, F.J. Gil Llambıas, Appl. Catal. A 322 (2007) 113–120.
[44] E. Desimoni, G.I. Casella, A.M. Salvi, T.R.I. Cataldi, A.A. Morone, Carbon 30 (1992) 527–531.
[45] H.W. Tien, Y.L. Huang, S.Y. Yang, J.Y. Wang, C.C.M. Ma, Carbon 49 (2011) 1550–1560.
[46] J.P.R. Vissers, S.M.A. Bouwens, V.H.J. de Beer, R. Prins, Carbon 25 (1987) 485–493.
[47] U. Zielke, K.J. Huttinger, W.P. Hoffman, Carbon 34 (1996) 983–998.
[48] H. Oliveira, D. Franceschini, F. Passos, J. Braz. Chem. Soc. 25 (2014) 2339–2349.
[49] S. Guo, S. Zhang, L. Wu, S. Sun, Angew. Chem. Int. 51 (2012) 11770–11773.
[50] G. Lagos, R. García, A. López Agudo, M. Yates, J.L.G. Fierro, F.J. Gil-Llambías, N. Escalona, Appl. Catal A: General 358 (2009) 26–31.
[51] R. Johnstone, J. Liu, L. Lu, D. Whittaker, J. Mol. Catal. A: Chem. 191 (2003) 289–294.
[52] C. Barroo, S.V. Lambeets, F. Devred, T.D. Chau, N. Kruse, Y. De Deckerbc, T. Visart de Bocarmé, New J. Chem. 38 (2014) 2090–2097.
[53] Y. Wanga, Y. Denga, F. Shi, J. Mol. Catal. A: Chem. 395 (2014) 195–201.
[54] D. Teschner, J. Borsodi, Z. Kis, L. Szentmiklósi, Z. Révay, A. Knop-Gericke, R. Schlögl, D. Torres, P. Sautet, J. Phys. Chem. C 114 (2010) 2293–2299.
[55] A. Getsoian, Z. Zhai, A. Bell, J. Am. Chem. Soc. 136 (2014) 13684–13697.
[56] J.K. Nørskov, F. Abild-Pedersen, F. Studt, T. Bligaard, Proc. Nat. Acad. Sci. U. S. A. 108 (2011) 937–943.
[57] L. Kristinsdóttir, E. Skúlason, Surf. Sci. 606 (2012) 1400–1404.